8534 *Macromolecules* **2009**, *42*, 8534–8542
DOI: 10.1021/ma901486q

Macromolecules
ARTICLE

Molecular Dynamics Simulation of Intramolecular Cross-Linking of BCB/Styrene Copolymers

J. W. Liu,[†] M. E. Mackay,[‡] and P. M. Duxbury*,[†]

[†]*Department of Physics and Astronomy, Michigan State University, East Lansing, Michigan 48824, and* [‡]*Department of Materials Science, University of Delaware, Newark, Delaware 19716*

Received July 9, 2009; Revised Manuscript Received September 28, 2009

ABSTRACT: Polymeric nanoparticles can be manufactured by intramolecular cross-linking of benzocyclobutene (BCB)/styrene copolymers. We study this process by extensive molecular dynamics simulations of both atomistic and coarse-grained models. It is found that the rate of intramolecular cross-linking is close to quadratic in the number of unlinked cross-linkers, namely BCB monomeric units, while the completeness of the reaction is affected by the steric hindrance of the cross-linked polymer. An equation incorporating both of these processes yields a good agreement with simulation data. A rigidity effect is identified when the cross-linkers account for more than about 60% of a precursor BCB/styrene copolymer. Above this threshold, the radii of gyration of intramolecularly cross-linked BCB/styrene copolymers show little dependence on their cross-linker concentrations, and a relatively large number of BCB monomeric units are left unreacted in each polymer. In addition, a temperature series study is performed on the intramolecular cross-linking of freely jointed chain (FJC) samples. We introduce the chemical distance density to provide a relation between the topology of cross-linking and the structure of a cross-linked polymer. A power law relation is found between the radius of gyration of the polymer and the chemical distance density, in both FJC samples and BCB/styrene copolymers.

1. Introduction

The intramolecular cross-linking of a polymer is a process in which chemically active monomeric units react with one another to form additional covalent bonds. Active monomeric units are referred to as "cross-linkers" to distinguish them from monomeric units that cannot cross-link. The intramolecular cross-linking process permanently alters the structure of a polymer. As the density of intramolecular cross-links increases, a polymer becomes more compact and eventually transforms into a particle-like object. The feasibility of synthesizing nanoparticles by intramolecular cross-linking of polymers has been demonstrated in several recent experiments,[1−5] opening the door to fabrication of designed nanoparticles by cross-linking of carefully controlled unimolecular precursors.

Nanoparticles have abundant applications, such as biointegration,[6] polymer nanocomposite materials,[7] drug delivery,[8] stabilization of polymer films,[9,10] facilitation of polymer processing,[11,12] and so on. Those applications typically rely on nanoparticles with specific chemical and physical properties, which entails the ability to customize nanoparticles. Moreover, industrial production of nanoparticles requires an effective control over the manufacturing process. Therefore, a good understanding of the intramolecular cross-linking process is indispensable for its application to nanoparticle manufacturing.

Multiple factors can be utilized to direct intramolecular cross-linking processes. The percentage of cross-linkers in a precursor polymer is a first example, as it is easily tuned yet has a direct impact on the structure of the polymer nanoparticle end product. A polymer with more cross-linkers is more rigid, and usually, though not always, it is also more compact. The percentage of cross-linkers also affects other aspects of the cross-linking process including the reaction rate and the fraction of cross-linkers that are never able to find a partner, i.e., the reaction completeness.

*To whom correspondence should be addressed.

Polymers assume various morphologies under different environmental conditions, which can also play a role in the intramolecular cross-linking process. A single polymer can have two distinct morphologies, i.e., that of a compact globule or of an expanded coil. It can transform from one state to the other on changing either the ambient temperature or the quality of the solvent. Intuitively, when a polymer is in the globule state, the cross-links are more likely to form between well-separated cross-linkers, resulting in a more compact nanoparticle. However, when the polymer is in the coil state, the cross-links tend to occur between neighboring cross-linkers so that a more loosely cross-linked nanoparticle is formed. This fact was briefly acknowledged in previous works;[13,14] however, a systematic study of the effect of initial morphologies on intramolecular cross-linking of polymers is not available.

Intramolecular cross-linking of a polymer bears some resemblance to the folding of a protein as both of them involve the collapse of chains due to the interaction between their segments. In particular, the rigidity effect has been studied in protein folding processes.[15] One can expect that the rigidity of a polymer has a similar dependence on its intramolecular cross-linking density, as demonstrated here where we explore the conditions under which the rigidity transition may occur due to irreversible cross-linking.

In this paper, intramolecular cross-linking of polymers is explored by extensive molecular dynamics simulations, which were carried out using the LAMMPS software.[16] A letter outlining some of our results has recently appeared.[17]

Our simulation work was motivated by a recent experiment on the intramolecular cross-linking of BCB/styrene copolymers,[1] where it was demonstrated that nanoparticles with radii of gyration ranging from 5 to 20 nm can be manufactured by the intramolecular cross-linking of BCB/styrene copolymers. The experiment was performed in a good solvent so that the precursor polymers achieved expanded morphologies. A typical precursor polymer in the experiment consisted of 1000 monomeric

 Published on Web 10/08/2009

units, among which about 20% were BCB units. When heated to 250 °C, the BCB units started reacting with one another to form cross-links. The cross-linked polymers exhibited considerable contraction and formed nanoparticles eventually.

In practice, two different types of cross-linking can occur in a cross-linking experiment, namely intramolecular and intermolecular cross-linking. Intramolecular cross-linking connects monomeric units within a single polymer, while intermolecular cross-linking connects monomeric units from different polymers.

The key point of an intramolecular cross-linking experiment is to suppress unwanted intermolecular cross-linkings. Typically, this can be accomplished by reducing the concentration of polymers in the solution so that an ultradilute solution is often required for the ideal effect. In the ultradilute solution, it is very unlikely for two polymers to come close enough to form an intermolecular cross-link. However, in the ultradilute solution there is only a very small amount of the reactants, i.e., the precursor polymers, so this approach is not suitable for mass production.

Another technique, the "slow addition method", was introduced to address this difficulty.[1] In this procedure, the precursor polymers were added into the reaction container slowly, to allow enough time for each individual polymer to cross-link in isolation. At any time during the process, the concentration of the precursor polymers was kept low enough to ensure that intermolecular cross-linking was unlikely to occur. The concentration of final polymeric nanoparticle product increased steadily as the experiment went on and the nanoparticles could not react with each other as nearly all of their BCB units were engaged in intramolecular cross-linking.

Compared to the approach of cross-linking the polymer in an ultradilute solution, the slow addition method has obvious advantages. It requires much less solvent yet yields highly concentrated products. However, its applicability depends on the number of cross-linkers that are left unreacted as unreacted cross-linkers in a nanoparticle may lead to cross-linking with nanoparticles that are formed later. The concept cannot work in the case where a considerable number of cross-linkers are unable to find a partner. In the simulation we also inspected the number of unlinked cross-linkers to check the viability of the slow addition method.

This paper is organized as follows. In section 2, we introduce two models for our simulation study of intramolecular cross-linking: a united atom model and a freely jointed chain model. The simulation schemes for both models are also described. In section 3, the key results of the two models are presented. For the united atom model, we focus on the cross-linking reaction rate, the number of unlinked cross-linkers, and the rigidity of the cross-linked polymers. Simple theoretical analysis is also provided to help understand the systematics of the data. For the FJC model, we performed a temperature series of simulations to study the effect of initial morphologies on the cross-linking process. Since the quality of the solvent can also induce a change in morphology of the precursor polymer, the result of the temperature series simulation is also meaningful to the cross-linking experiments in various solvents at least to a first-order approximation. We then define the chemical distance density to describe the cross-linking topology of a cross-linked polymer. Its relation to the radius of gyration of the cross-linked polymer is elucidated. In the last section, we summarize our simulation studies and the overall understanding derived from them.

2. Models and Simulation Methods

United Atom Model. The structure of a BCB/styrene copolymer is very similar to that of a polystyrene polymer. The only difference between them is that the former contains BCB units, with each BCB unit being a styrene with two extra CH units. Hence, it is not difficult to derive an atomistic model for BCB/styrene copolymer based on existing models for polystyrene.

Because of its importance as a model polymer, there have been many simulation studies of polystyrene, and a variety of atomistic models have been employed. Among them, we chose a united atom model of polystyrene[18] as it provides a balance between computational efficiency and accuracy. This model was shown to yield good agreement with X-ray and neutron diffraction data, and recent simulations of polystyrene using this model also proved to be successful.[19−22] The model treats a carbon atom with its bonded hydrogen atoms as a single particle, i.e., a united atom, and incorporates a widely used united atom force field.[23] Though this force field has been considerably updated in the past few decades,[24−27] the original version is still in use and is valid for molecular dynamics simulations in vacuum.

Our simulations were also performed in vacuum, though the experiment[1] was done in a good solvent with temperature $T =$ 523 K where the precursor polymers assumed expanded coil morphologies. The morphology of the precursor polymer is important to the final structure of cross-linked nanoparticles, and in order for polymers to achieve similar morphologies in vacuum, a high temperature ($T = 900$ K) was used for our simulations. We have carried out a simulation study of the radius of gyration of polystyrene chains with $N = 500$ monomers. In these calculations we started the simulation at a low temperature ($T = 480$ K) where the polymer is in the globule state and increased the temperature linearly from this starting temperature to a final temperature of 1500 K, where the polymer is in the coil phase. This heating process consisted of 5 million timesteps. Averaging the results over ten trials provides a clear picture of the coil globule transition, which starts at ~750 K and is complete at ~1000 K. The temperature chosen for our cross-linking simulations is 900 K, that is, in the coil−globule transition regime of this atomistic model. In reality, polystyrene cannot survive such high temperatures; however, the correspondence between polymer mophology at high temperature in vacuum and polymer morphology at lower temperature in good solvent is a commonly used device in comparison between theory and experiment. In many ways, the temperature in our simulations can be viewed as an effective temperature which incorporates the effects of both the solvent and the experimental temperature.

We slightly modified the original polystyrene force field to adapt to the simulation software LAMMPS.[16] First, we used harmonic potentials to describe bond stretching interactions between united atoms, while in the original model the bond lengths were constrained by the SHAKE algorithm. The strengths of the potentials for bond stretching interaction were taken from experimental data, but they were reduced by a factor of 4 to increase the simulation time step.[28] Second, the original model incorporated dihedral potentials between atoms of a phenyl in order to maintain its planar configuration. But in our simulation a phenyl was constrained as a rigid body so that its six united atoms moved uniformly as a whole. The total force on a phenyl was calculated as the sum of all external forces on its six united atoms. This treatment of phenyls has two advantages. Not only can it maintain a strict planar configuration for the phenyls, it can also speed up the computer simulation because all the internal forces within the rigid body do not need to be considered. Similar rigid body constraints were also used for benzocyclobutenes in BCB units, where each BCB unit consisted of eight united atoms. Other details of the polystyrene force field were taken from the literature.[18]

Table 1. Parameters of the Force Field for the United Atom Model of a BCB/Styrene Copolymer[a]

Lennard-Jones		
CH_2	$\varepsilon = 0.12$	$\sigma = 3.85$
CH	$\varepsilon = 0.09$	$\sigma = 3.7$
C(ar), C(ar)H	$\varepsilon = 0.12$	$\sigma = 3.7$
	cutoff distance = 7.65	
bond		
C−C	$K_r = 80$	$r_0 = 1.54$
C(ar)−C	$K_l = 80$	$l_0 = 1.50$
angle		
C−C(ar)−C(ar)	$K_\alpha = 70$	$\alpha_0 = 120$
C−C−C	$K_\theta = 60$	$\theta_0 = 109.5$
dihedral		
backbone	$K_\phi = 1.4$	
phenyl rotation	$K_\psi = 1.0$	
improper		
C(ar)	$K_\omega = 80$	$\omega_0 = 0$
C	$K_\chi = 50$	$\chi_0 = 35.26$

[a] Energy is in kcal/mol, distance is in Å, and angle is in deg.

The force field in our simulations took the following forms:

$$E_{LJ} = 4\varepsilon\left[\left(\frac{\sigma}{r}\right)^{12} - \left(\frac{\sigma}{r}\right)^{6}\right]$$

$$E_{bond} = K_r(r - r_0)^2 + K(l - l_0)^2$$

$$E_{angle} = K_\theta(\theta - \theta_0)^2 + K_\alpha(\alpha - \alpha_0)^2$$

$$E_{dihedral} = K_\phi(1 + \cos(3\phi)) + K_\psi(1 - \cos(2\psi))$$

$$E_{improper} = K_\chi(\chi - \chi_0)^2 + K_\omega(\omega - \omega_0)^2$$

The parameters in the above equations are listed in Table 1. Lennard-Jones interactions between united atoms separated by four or more bonds are considered in the simulations.

The simulations were carried out for BCB/styrene copolymers with 250, 500, and 750 monomeric units separately. Unlike the experiments where the BCB concentration was below 30%, we varied the percentage of BCB units from 5% to 100% to investigate the full range of cross-linker concentrations. Ten samples were studied for each size and each cross-linker concentration, and the results were averaged to get better estimates of properties.

The initial configuration for a BCB/styrene copolymer was generated in three steps. First, its backbone was created by a self-avoiding walk (SAW) on a diamond lattice. Each site of the walk represented a CH_2 or a CH united atom alternatively. The diamond lattice automatically ensured that two neighboring bonds made an angle of 109.5°. In the second step, we attached side groups to the CH united atoms. There were two types of side groups, phenyl and BCB, with different populations. They were added in a totally random manner, with BCB concentration being x. Each side group can be attached to any CH united atom and can be on either side of the backbone, so the polymer that is generated is an atactic random copolymer. However, newly added side groups can be too close to other particles of the polymer so we ran a short preliminary NVT simulation for the polymer to resolve any dangerous configurations. In this simulation a soft pair potential was temporarily imposed for all unit atoms in order to push close pairs apart. The preliminary NVT simulation lasted for only a few picoseconds and lead to expanded morphologies for all samples.

Simulation of intramolecular cross-linking of BCB/styrene copolymers began with the initial configurations generated as described above and consisted of three stages: equilibration, cross-linking, and re-equilibration. In the equilibration stage, NVT simulations of all samples were run for 3.2 ns at 900 K. In the subsequent cross-linking stage, we ran the same NVT simulations; however, they were paused every 0.8 ps to check if the cross-linking criteria could be met. At each check, we examine the distances between all pairs of BCB units, in particular, the distances were measured from C_1/C_2 of one BCB unit to C_3/C_4 of another BCB unit, as shown in Figure 1. To establish a C_1 bond to C_3 and C_2 to C_4 we require their distances to be less than 5 Å, or approximately 1.3σ, where σ is the hard-core radius of the Lennard-Jones interaction between two CH united atoms. This distance requirement is consistent with previous bulk cross-linking simulations.[29] We also considered the relative orientation of two BCB units, so that new chemical bonds were only formed when the four active carbon united atoms C_1, C_2, C_3, and C_4 approached each other in a way that their orbital electron clouds overlapped significantly. To impose this condition, four angles were examined as listed in Table 2. All of these angles have equilibrium values of 109.5°, and in the simulation we required their values to be more than 90° and less than 130° in order for the cross-linking reaction to proceed.

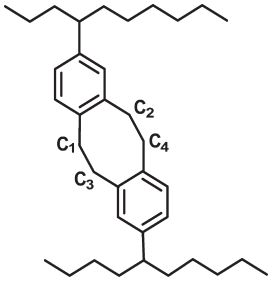

Figure 1. Cross-link between two BCB units.

Table 2. Table of the New Bond in Cross-Link

bond	C_1-C_3	C_2-C_4
angle	C(ar)−C_1−C_3 C(ar)−C_2−C_4	C_1−C_3−C(ar) C_2−C_4−C(ar)
dihedral	C(ar)−C_1−C_3−C(ar) C(ar)−C_2−C_4−C(ar)	

As shown in Figure 1, the cross-link between two BCB units is a floppy eight-membered ring that introduces a number of extra bonded interactions to the model. These interactions are listed in Table 2. In total two covalent bonds, four angle potentials and two dihedral potentials are added for each new cross-link, and the force field of a new cross-link is the same as that of the backbone of a BCB/styrene copolymer.

The check for the reaction criteria was performed every 0.8 ps in our simulations. This interval was long enough to allow for the configuration of a polymer to undergo a nontrivial change, yet it was short enough for the simulated cross-linking to be finished in a reasonable computation time. Once a pair of BCB units was found to meet the reaction criteria, the cross-link formed immediately between them. Though formation of a cross-link provides a significant perturbation to the system, the time step used in the simulations was sufficiently small to ensure that the simulation proceeded in a stable manner without further intervention. The cross-linking stage lasted until there were less than two BCB units left in a polymer or until 17 ns simulation time elapsed, whichever occurred first.

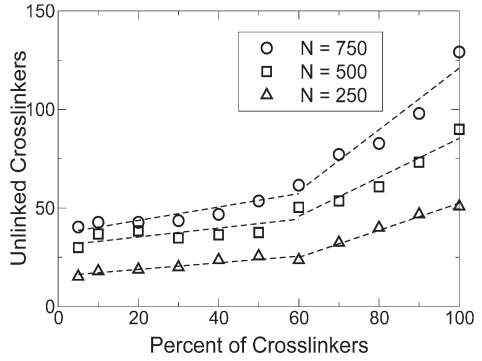

Figure 2. Final number of unlinked cross-linkers for polymers with 250, 500, and 750 monomeric units after 17 ns of cross-linking. They have different linear dependences on the cross-linker concentration below and above 60% cross-linkers.

Once the cross-linking ceased, the last stage consisted of a re-equilibration process for another 3.2 ns. The cross-linked polymers were then analyzed.

Freely Jointed Chain (FJC) Model. The force field of the FJC model in our simulation is

$$E = \sum_{\text{pairs}} 4\varepsilon\left[\left(\frac{\sigma}{r}\right)^{12} - \left(\frac{\sigma}{r}\right)^{6}\right] + \sum_{\text{bonds}} K(r - r_0)^2 \qquad (1)$$

where $\varepsilon = 1$, $\sigma = 1$, $K = 1000$, and $r_0 = 1$ in Lennard-Jones units. The cutoff distance for the Lennard-Jones interaction in this model is 3. Stiff polymers can be modeled as freely jointed chains in which each segment represents m ($m > 1$) monomeric units. The segment length m is known as Kuhn length. The FJC model therefore can approximate a polystyrene chain providing that one of its beads represents 7 monomeric units, namely the Kuhn length of polystyrene.[30]

In our simulation, each FJC sample comprised of 500 beads, of which a fraction, x, were cross-linkers while the remainder were normal beads. Aside from its ability to cross-link, a cross-linker is the same as a normal bead, with both interacting through the force field defined in eq 1. We studied four different concentrations of cross-linkers, namely 5%, 20%, 50%, and 100%.

A temperature series simulation is performed on the FJC model to study the effect of the initial morphology of a polymer on its intramolecular cross-linking. The temperatures considered were in the range $T = 0.5$ to $T = 11$ (also in Lennard-Jones units), which covered all the temperature points of interest for our FJC model. In particular, more points were taken between $T = 3$ and $T = 5$, which lie in the coil globule transition regime, and in total 44 temperature points were considered. At each temperature point, 50 FJC samples were studied for each of the four cross-linker concentrations mentioned previously, so the total number of FJC samples studied was $50 \times 4 \times 44 = 8800$.

First, the initial configurations of the FJC samples at the highest temperature $T = 11$ were generated. The chains were constructed by using self-avoiding walks on FCC lattices with lattice constant $a = 1$, and the cross-linkers of each sample were randomly distributed over the chain. The initial configurations for the samples at lower temperatures were simply copied from the equilibrated samples at the next higher temperature; e.g., the initial configurations of the FJC samples at $T = 10$ were obtained from the FJC samples after equilibration at $T = 11$. Note that in this copy procedure the locations of cross-linkers were rearranged randomly, so that the initial cross-linker configuration for a sample at lower temperature had a new sequence.

A simulation of the intramolecular cross-linking of the FJC model was similar to that of the atomistic model of BCB/styrene copolymers described above. It also consisted of equilibration, cross-linking, and re-equilibration stages. In the equilibration process, NVT simulations were run for 10000τ, where $\tau = (m\sigma^2/\varepsilon)^{1/2}$ is the Lennard-Jones time unit. Subsequently, the cross-linking process was carried out and consisted of 9000τ, with the interval between checks for the cross-linking criteria being 10τ. Unlike the atomistic model, there was no need to check for the orientation between two cross-linkers. The only condition to be met for two cross-linkers to react was that their distance should be less than 1.3σ. Again, the time step was small enough to ensure that even after a cross-linking event the simulation remained stable. The final re-equilibration process consisted of NVT simulations for 10000τ.

3. Results

Cross-Linking Reaction of BCB/Styrene Copolymers. The simulated reaction rate of the intramolecular cross-linking of a BCB/styrene copolymer is greatly restrained by both orientation and distance requirements for two BCB units. For instance, the simulation shows that it takes about five checks on average to form a cross-link in a polymer with 750 unlinked BCB units, which corresponds to a reaction rate at the picosecond time scale. Moreover, the reaction rate drops quickly as the number of unlinked BCB units decreases and is at the nanosecond time scale when there are only tens of unlinked BCB units left.

Because of its slow kinetics, the simulation of the intramolecular cross-linking of a BCB/styrene polymer cannot be completed in a practical computing time so we set a time limit of 17 ns on the cross-linking simulations. It is found that a majority of cross-linkers are able to cross-link within this time period though a substantial number of them remain unlinked. In Figure 2, the number of unlinked cross-linkers remaining after 17 ns as a function of BCB concentration is plotted for polymers of three sizes (N = 250, 500, and 700). An interesting observation is that the data exhibit different behaviors below and above 60% of cross-linkers. In both regions the number of unlinked cross-linkers has an approximately linear dependence on the cross-linker concentration; however, there is a change in slope at about 60% cross-linkers.

In addition, there are no obvious signs that the reactions are complete even though they are proceeding at extremely slow rates at longer times. Theoretically, we would like to know if all cross-linkers can be cross-linked, which also has significance to the real applications. For example, unreacted cross-linkers can function as docking points in drug delivery, and they also affect the applicability of the slow addition method used in synthesis of the nanoparticles. To estimate the asymptotic number of unlinked cross-linkers, we studied the cross-linking kinetic data presented in Figure 3.

The cross-linking of two BCB units is an elementary reaction that is approximated by the law of mass reaction, namely the reaction rate is proportional to the product of concentrations of reactants. In a previous study it has been applied to end-linked polymers.[31] In our system the first-order approximation to the number of remaining cross-linkers is given by the equation

$$\mathrm{d}x(t)/\mathrm{d}t = -kx^2(t) \qquad (2)$$

where $x(t)$ denotes the number of unreacted cross-linkers at time t and k is a rate constant. Note that in eq 2 we use the numbers of reactants, i.e., cross-linkers, instead of their

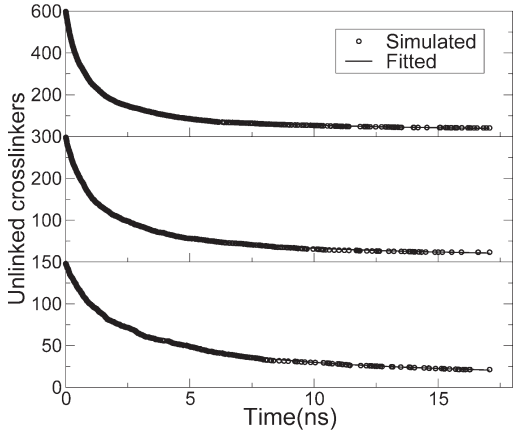

Figure 3. Number of unlinked cross-linkers for BCB/styrene copolymers with 750 monomeric units decreases as the cross-linking simulation proceeds. From the top down, the three panels are for 80%, 40%, and 20% BCB units, respectively.

concentrations. As a consequence, the coefficient k should contain an additional factor of $1/V$ with V being the reaction volume. Since the intramolecular cross-linking occurs only in the vicinity of a polymer, the reaction volume is proportional to the polymer size. By multiplying by the number of monomeric units N, a normalized coefficient can be obtained which is $k^* = kN$.

The solution to eq 2 is

$$x(t) = \frac{x(0)}{1+At} \tag{3}$$

where $A = kx(0)$. This solution predicts that the number of free cross-linkers decays slowly with time and goes to zero at long times. However, this simple model omits the influence of steric hindrance on the reaction rate. In particular, if cross-linking produces a highly constrained or rigid nanoparticle, it may be impossible for some cross-linkers to find a partner. As a result, there can be some free cross-linkers left unreacted even if the cross-linking runs for an infinitely long time.

To approximate the effect of the steric hindrance on cross-linking, eq 2 is generalized to

$$x(t) = \frac{x(0)}{B+At} + x_\infty \tag{4}$$

where x_∞ is the number of cross-linkers that are left unreacted eventually. The unity in the equation is replaced with a parameter B in order to maintain its validity when t goes to zero.

This equation provides an excellent representation of all of the simulation data that we have obtained, except at really low cross-linker concentrations where strong statistical variations render the fitting less reliable. Examples of fits to the data for three different cross-linker concentrations, 80%, 40%, and 20% are presented in Figure 3. In these graphs all samples have 750 monomeric units.

From these fits, we find values for the parameters k^*, B, and x_∞ for all cross-linker concentrations but 5%, which has large variations. The normalized coefficient k^* is shown in Figure 4a, demonstrating that k^* is approximately the same for all concentrations and all sizes. The parameters B and x_∞ are plotted in parts b and c of Figure 4, respectively. The parameter B assumes values close to unity, which is reasonable. However, the most interesting result is that x_∞ assumes larger values when the concentration of cross-linkers is above 60% and rises roughly linearly with cross-linker concentration beyond this point, in a manner very similar to the raw data presented in Figure 2. In the next subsection we attribute this behavior to a rigidity effect.

Rigidity Effect in Cross-Linked BCB/Styrene Copolymers. It is not surprising that higher levels of cross-linking yield more rigid nanoparticles. As noted in the previous subsection, this can lead to some unpartnered BCB units even at very long reaction times. We have also studied the radius of gyration of the cross-linked nanoparticles and find some rigidity effects in their behavior. First we note that the radius of gyration of a cross-linked BCB/styrene copolymer in the simulation is comparable to that in the experiment.[1] For instance, in the experiment a precursor polymer with molecular weight 11200 amu and 10% BCB units yields a nanoparticle with hydrodynamic radius $R_h = 6.2$ nm after cross-linking. This polymer has roughly 100 BCB units and 900 styrenes. In the simulations, the largest samples have 750 monomeric units. With 10% BCB units, they form nanoparticles with average radius of gyration $R_g = 5.3$ nm.

In Figure 5, the average radius of gyration found in simulations is plotted for BCB/styrene copolymers with three different sizes. It shows a decreasing trend with the increasing fraction of cross-linkers. However, when the BCB concentration is above 60%, the R_g curves cease to show any decrease.

In a previous work, we studied the rigidity effect on the intramolecular cross-linkings of polymers using coarse-grained models.[17] It was found that a rigidity transition occurred in some models with increasing cross-linker concentration. For example, the freely rotating chain (FRC) model exhibited a rigidity transition at 40% of cross-linkers. Above the rigidity transition, the R_g of cross-linked polymers showed little change with the cross-linker concentration, and the number of unlinked cross-linkers was higher. The Maxwell counting method[32] was employed to determine the rigidity transition threshold for the coarse-grained models, and nice agreement with simulations was achieved.

Since the united atom model for BCB/styrene copolymer is cumbersome for a rigidity analysis, it is clearer to use an associated FJC model and to apply the Maxwell counting technique to this associated model. Usually in the freely jointed chain (FJC) models, each segment contains only one bead which represents m monomeric units (for polystyrene $m = 7$). But in order to obtain the correct cross-linker concentration, we use one bead to represent a single monomeric unit, be it styrene or BCB, so that one segment should contain seven beads. They are distributed evenly along the whole segment and are strictly aligned in a straight line all the time.

Before cross-linking, the number of degrees of freedom in a stiff chain with N beads and segment length m is $2N/m$ since the chain is equivalent to a simple FJC with N/m beads where each bead has two unconstrained degrees of freedom. The number of cross-linkers is xN, where x is the cross-linker percentage. In the atomistic model, a cross-link between two BCB units brings about seven additional constraints. However, the only effect of those seven constraints on two BCB units is to limit their distances. Therefore, a cross-link adds only one effective constraint in the FJC model. Based on the Maxwell counting, the number of floppy modes F of the model can be written as

$$F(y) = 2\frac{N}{m} - \frac{xN}{2} \tag{5}$$

The rigidity transition should occur when F vanishes, yielding $x_c = 4/m$. Polystyrene has a Kuhn length $m = 7$,[30] which leads to the Maxwell counting estimate of the rigidity threshold $x_c = 4/7 \approx 57.14\%$.

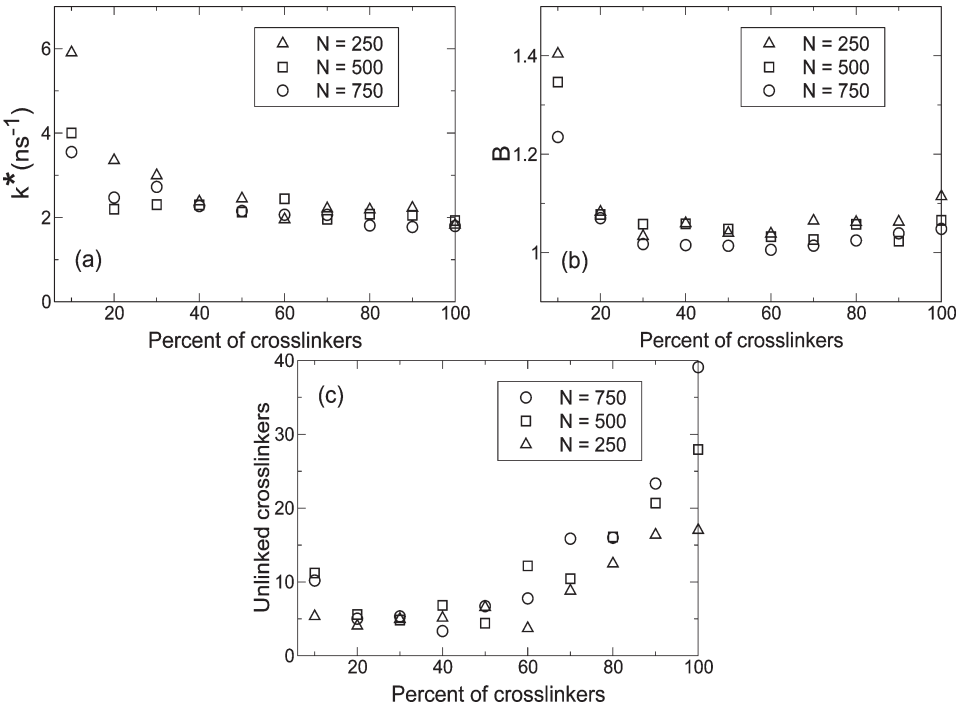

Figure 4. From top down, the parameters k^*, B, and x_∞ (unlinked cross-linkers) from fitting to eq 4 are plotted in each panel. The number of unlinked cross-linkers shows a rigidity effect at around 60% of BCB units.

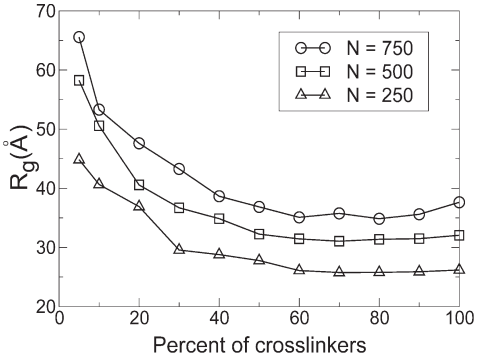

Figure 5. Radius of gyration for a cross-linked polymer is plotted for BCB/styrene copolymers. A rigidity effect is observed in a cross-linked BCB/styrene copolymer when the cross-linker concentration is above 60%.

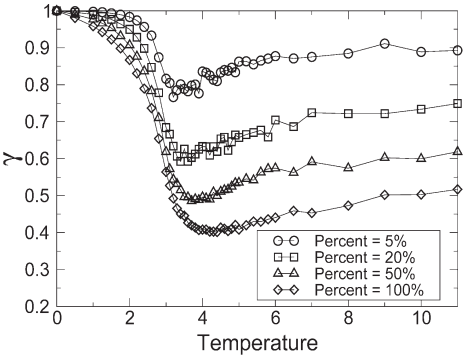

Figure 6. Average contraction ratio γ, consisting of the ratio of the radius of gyration of the polymer after and before cross-linking, as a function of the cross-linking temperature. The four curves correspond to four different concentrations of cross-linkers.

On the other hand, based on the simulation data, the rigidity threshold for a cross-linked BCB/styrene copolymer is around $x_c = 60\%$, as seen in Figures 2 and 5. It is in good agreement with the Maxwell counting estimate, indicating that simple constraint counting ideas provide a good starting point for understanding rigidity effects in unimolecular cross-linking. It should be noted that the cross-links in polystyrene are flexible in the sense that they can rotate somewhat; however, they impose limits on the ability of the chain to fluctuate and in particular to extend. In technical terms they are closer to tensegrity constraints rather than pure rigid constraints. The Maxwell counting estimate above is then an upper estimate of the rigidity of the cross-linked polymer.

Contraction of FJC Samples. The contraction factor is defined as the ratio of the radius of gyration of a polymer after and before cross-linking, denoted as $R_g(x)$ and $R_g(0)$, respectively:

$$\gamma = \frac{R_g(x)}{R_g(0)} \tag{6}$$

In Figure 6 the contraction factor is plotted as a function of the cross-linking temperature, indicating that the largest contraction occurs between $T = 3.5$ and $T = 4$, which is just above the coil−globule transition and close to the Θ temperature of the FJC model used here.

In general, cross-linking results in a wide structural diversity in the final products because there are numerous ways to cross-link a chain with 500 beads. This is reflected in large fluctuations in the values of R_g especially at higher temperatures, leading to the relatively big fluctuations in γ above the Θ temperature for all curves in Figure 6. At lower temperatures, the starting state is already a globule so the effect of cross-linking on the size of the polymer decreases and fluctuations are smaller. The contraction of an intramolecularly cross-linked polymer is naturally related to its density of cross-links, and since all cross-linkers can find a partner in the FJC model, which has no rigidity effect, the density of cross-links in the final state is simply proportional to its cross-linker concentration. As evident in Figure 6, larger concentrations of cross-linkers lead to greater contractions

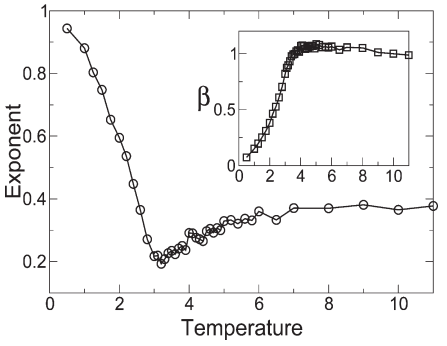

Figure 7. Simulation data for the contraction ratio $\gamma = R_g(x)/R_g(0)$ fitted to the expression $\gamma^2 = 1 - \beta\rho^e$ yields the values for the prefactor β and the exponent e plotted in the figure.

of the final states of FJC samples at all temperatures. This is counter to the effects observed in systems exhibiting a rigidity effect where contraction of polymers ceases to increase beyond the rigidity threshold.

An early work[13] studied the quantitative relation between R_g and the density of cross-links, in cases where the polymers are made completely of cross-linkers, i.e., $x = 1$. Using the ideal chain model, they argued that for a chain with N monomeric units and m cross-links the ensemble average of its contraction can be described by $\langle\gamma^2(N,m)\rangle = 1 - \beta\rho^{1/2}$, where $\gamma = R_g(x)/R_g(0)$ and $\rho = m/N$. This prediction was compared to experiments where the cross-linking reaction could be turned off before it was complete, enabling access to the full range of values of cross-link density. The density of cross-links ρ can then assume any value from 0 for a chain with no cross-links to 0.5 for a fully cross-linked chain. The theory agreed well with their experiments; however, the authors suggested that their theory cannot be applied to the intramolecular cross-linkings of chains with only a fraction of randomly distributed cross-linkers. The fundamental reason, they argued, is that the density of cross-links by itself is insufficient to describe the cross-link process, and instead the distribution of cross-linking rings is important. The radius of gyration depends on detailed information about all rings, particularly their number and their sizes. The more rings there are or the larger an individual ring is, the greater the contraction of the polymer is. However, for chains made of randomly distributed cross-linkers, the distribution of the cross-linking rings is difficult to evaluate because it depends strongly on the initial locations of cross-linkers.

In order to compare our simulation results for the contraction factor to the ideal model, we fitted the data to the generalized form $\gamma^2 = 1 - \beta\rho^e$, and the results are presented in Figure 7. The prediction based on the ideal chain model is $\beta \approx 0.75$, $e = 1/2$ and applies to the theta point that occurs at a temperature of approximately $T = 3.5$ for our FJC model. The exponent we find is considerably smaller than 1/2 though the prefactor is quite close to that predicted by the ideal theory, implying a stronger contraction effect than predicted by the ideal model. This is most likely due to the fact that the precursor chain is more expanded than the ideal chain because of hard-core repulsion effects. The nonmonotonic behavior in the exponent reflects the nonmonotonic temperature dependence of the contraction ratio (see Figure 6) and is due to a subtle interplay between the size of the precursor chain and the number of large rings that are produced by cross-linking.

Chemical Distance Density. To further quantify the effect of the size of cross-linking rings on the structure of the

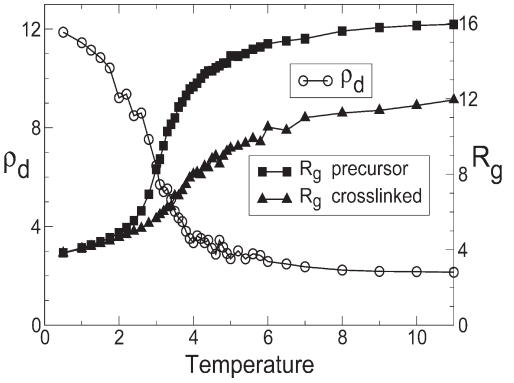

Figure 8. Chemical distance density and radius of gyration R_g, both before and after cross-linking, are plotted for different temperatures. This data is for FJC chains with $N = 500$ and $x = 20\%$.

cross-linked polymer, we introduce the "chemical distance" as the number of monomeric units (along the chain backbone) that separate two monomeric units that form a cross-link. And the chemical distance density is defined as

$$\rho_d = \frac{\sum_{i=1}^{m} d_i}{N} \tag{7}$$

where d_i is the chemical distance for the ith cross-link and N is the total number of monomeric units in a polymer. The summation runs over all the cross-links. Chemical distance density indicates the overall effect of the cross-linking rings, incorporating both their number and their sizes. It can serve as a useful measure of the structure of an intramolecularly cross-linked polymer. The largest value of ρ_d is of the order of the number of monomeric units N. For example, when every monomeric unit i ($1 \le i \le N/2$) is connected to a monomeric unit $N/2 + i$, yielding a chemical distance of $N/2$, the chemical distance density of the cross-linked polymer acquires a value of $N/4$. It is also convenient to extend the definition of the chemical distance to a linear polymer, where each pair of connected monomeric units contributes a chemical distance of unity, and its chemical distance density is also approximately unity.

The data of Figure 8 show that the chemical distance density has a clear temperature dependence, assuming large values in the globule region and becoming quite small in the coil region. And there is a sharp decline of the chemical distance density at the coil−globule transition regime.

To find a quantitative relation between the chemical distance density and the radius of gyration, we examined the simulation data at each temperature point separately. By doing so, the temperature effect on the radius of gyration can be excluded from the analysis. At each temperature point there are four different cross-linker concentrations and 50 samples for each concentration. This yields 200 data points for R_g and chemical distance density. On the basis of analysis of this data, we find that R_g has a power law dependence on chemical distance density (see Figure 9):

$$R_g = R_g(0)(1+\rho_d)^g \tag{8}$$

Unity is added to ρ_d in eq 8 to recover the correct limit of the precursor chain. The exponent g in eq 8 extracted from fits such as those in Figure 9 is temperature-dependent, but it is not dependent on the cross-linking fraction because the effect of cross-linking is captured by the chemical distance density ρ_d.

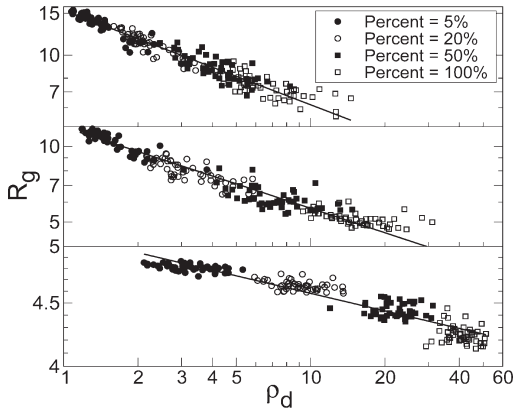

Figure 9. Equation 8 is fitted to the simulation data for FJC models at different temperatures. Starting from the top the data is for cross-linking temperatures $T = 8$, 4, and 2, respectively.

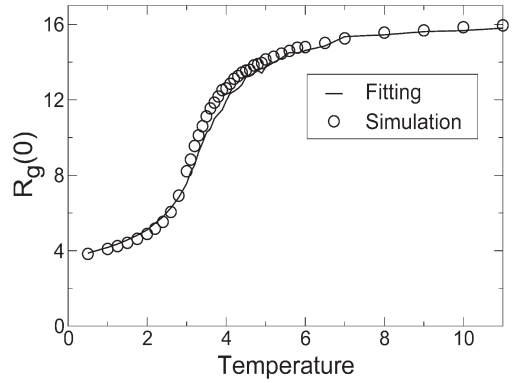

Figure 10. Radius of gyration before cross-linking found from fitting of the cross-linked FJC samples to eq 8 compared to the simulation data, showing good agreement.

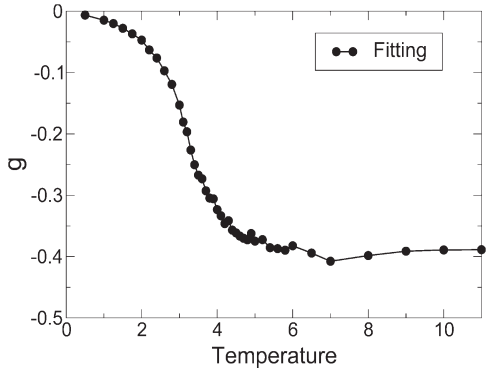

Figure 11. Exponent g in eq 8 for a FJC model is obtained from fittings at all temperatures. Note that the exponent is independent of the cross-link density.

A series of values for $R_g(0)$ and for g at each temperature are obtained from the fitting procedure illustrated in Figure 9, where $R_g(0)$ is the radius of gyration of a polymer before cross-linking. As shown in Figure 10, $R_g(0)$ obtained from the fitting procedure agrees well with that found directly from simulations. The exponent g in eq 8 is plotted in Figure 11. It changes smoothly from the low temperature ($T = 0.5$) to the high temperature ($T = 11$) where g is approximately -0.4. Overall, eq 8 turns out to be a good fit to the simulation data, though some deviations can be seen for large chemical distance densities and at low temperatures. A large chemical distance density implies that there are

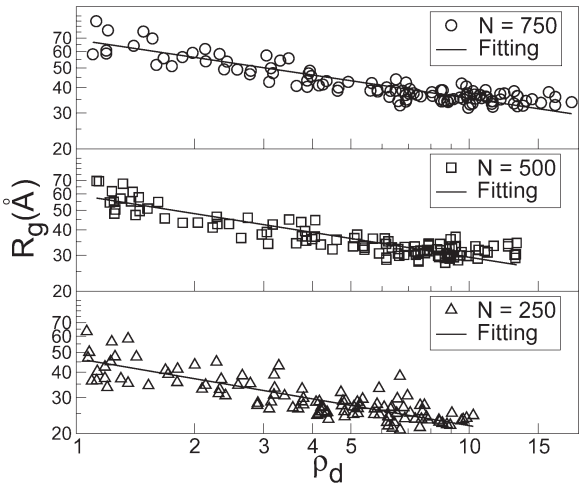

Figure 12. Radius of gyration as a function of chemical distance density for intramolecularly cross-linked BCB/styrene copolymers is plotted. From top down, three panels are for samples with 750, 500, 250 monomeric units, respectively. In each panel, the data (open symbols) and the fit to eq 8 (solid line) are shown.

complicated interpenetrating ring structures in the intramolecularly cross-linked polymer and is most pronounced at low temperatures where the precursor polymers are in a compact state even prior to cross-linking.

We also tested whether the power law relation of eq 8 applies to the intramolecularly cross-linked BCB/styrene copolymers. As we have described before, the simulations were performed for samples with 250, 500, and 750 monomeric units, and for each size, 11 concentrations from 5% to 100% were studied. For each concentration, we studied 10 samples, so that in total there were 110 samples for each size. Equation 8 was then used to fit the data as presented in Figure 12. Fitting yields good agreement except for a few data points with large chemical distance densities.

To compare the FJC results with those for the BCB/styrene copolymer, we consider that one FJC bead represents about seven BCB/styrene units.[30] A 500-bead FJC sample in the temperature series simulation then approximates a BCB/styrene copolymer with 3500 monomeric units. Second, the simulation of the atomistic model is performed at $T = 900$ K, which is near the coil−globule transition temperature for the atomistic model in vacuum, so the corresponding Lennard-Jones temperature for the FJC model is between $T = 3$ and $T = 4$, namely its coil globule transition regime. The exponent g for the FJC model ranges from -0.25 to -0.35 in this regime. Data extracted from simulations of the atomistic BCB/styrene model lead to values of $g = -0.33$, -0.31, and -0.29 for $N = 250$, 500, and 750 monomeric units, respectively, which are consistent with each other and with the FJC model results.

4. Summary

We carried out a simulation study of intramolecular cross-linking of BCB/styrene copolymers using an atomistic model. In addition, freely jointed chain models were adopted for a rigidity analysis and for temperature series simulations. Various factors that can affect the cross-linking and the size of the cross-linked end state were considered, including the concentration of cross-linkers, the ambient temperature, and the rigidity effect.

Simulations of the atomistic model of BCB/styrene copolymers show that over a wide regime the cross-linking rate has a quadratic dependence on the number of free cross-linkers. However, steric hindrance plays an important role in the intramolecular cross-linking, where it may prevent a finite fraction of

cross-linkers from being cross-linked even at long times. An equation incorporating both the quadratic dependence and the steric hindrance provides a successful description of the cross-linking reaction.

A rigidity transition occurs in the intramolecular cross-linking of BCB/styrene copolymers when the BCB concentration is above 60%. In this region, the number of unsatisfied cross-linkers goes up considerably. Moreover, in this regime, R_g of the cross-linked copolymers exhibits little change with increasing number of cross-links. We applied the Maxwell counting method to the stiff FJC model of BCB/styrene copolymers and found the quantitative dependence of its rigidity threshold on its Kuhn length.

We showed that the morphologies of the precursor polymers greatly affect their intramolecular cross-linking. The change of the morphology of a polymer can be induced by ambient temperature or by the quality of its solvent, providing experimental control of the effect. The key qualitative effect is that cross-linking of polymers from precursors in the globule state yields a tightly interconnected particle, while cross-linking from a precursor in the coil state leads to a relatively loose particle.

The chemical distance density was introduced as a useful measure of the internal structure of a cross-linked polymer. It provides a better account of the contraction of a cross-linked polymer than the density of cross-links, particularly for a polymer with randomly distributed cross-linkers. A systematic simulation using FJC chains shows that there exists a power law relation between the R_g and the chemical distance density. The exponent of the power law relation is determined for a series of temperatures by fitting and approaches $g \approx -0.4$ in the high temperature limit. A power law relation between R_g and the chemical distance density is also found for the atomistic model of BCB/styrene copolymers. In the coil−globule transition regime of this model, and of the FJC model, the exponent g is approximately -0.3.

Acknowledgment. This work was supported by the Center for Nanomaterials Design and Assembly at Michigan State University.

References and Notes

(1) Harth, E.; Horn, B. V.; Lee, V. Y.; Germack, D. S.; Gonzales, C. P.; Miller, R. D.; Hawker, C. J. *J. Am. Chem. Soc.* **2002**, *124*, 8653–8660.
(2) Mecerreyes, D.; Lee, V.; Hawker, C. J.; Hedrick, J. L.; Wursch, A.; Volksen, W.; Magbitang, T.; Huang, E.; Miller, R. D. *Adv. Mater.* **2001**, *13*, 204–208.
(3) Jiang, J.; Thayumanavan, S. *Macromolecules* **2005**, *38*, 5886–5891.
(4) Aliyar, H. A.; Hamilton, P. D.; Remsen, E. E.; Ravi, N. *J. Bioact. Compat. Polym.* **2005**, *20*, 169–181.
(5) Beck, J. B.; Killops, K. L.; Kang, T.; Sivanandan, K.; Bayles, A.; Mackay, M. E.; Wooley, K. L.; Hawker, C. J. *Macromolecules* **2009**, *42*, 5629–5635.
(6) Katz, E.; Willner, I. *Angew. Chem., Int. Ed.* **2004**, *43*, 6042–6108.
(7) Balazs, A. C.; Emrick, T.; Russell, T. P. *Science* **2006**, *314*, 1107–1110.
(8) Rosler, A.; Vandermeulen, G. W. M.; Klok, H. A. *Adv. Drug Delivery Rev.* **2001**, *53*, 95–108.
(9) Krishnan, R. S.; Mackay, M. E.; Duxbury, P. M.; Pastor, A.; Hawker, C. J.; Van Horn, B.; Asokan, S.; Wong, M. S. *Nano Lett.* **2007**, *7*, 484–489.
(10) Mackay, M. E.; Tuteja, A.; Duxbury, P. M.; Hawker, C. J.; Van Horn, B.; Guan, Z. B.; Chen, G. H.; Krishnan, R. S. *Science* **2006**, *311*, 1740–1743.
(11) Mackay, M. E.; Dao, T. T.; Tuteja, A.; Ho, D. L.; Van Horn, B.; Kim, H. C.; Hawker, C. J. *Nat. Mater.* **2003**, *2*, 762–766.
(12) Tuteja, A.; Duxbury, P. M.; Mackay, M. E. *Macromolecules* **2007**, *40*, 9427–9434.
(13) Martin, J. E.; Eichinger, B. E. *Macromolecules* **1983**, *16*, 1345–1350.
(14) Antonietti, M.; Sillescu, H.; Schmidt, M.; Schuch, H. *Macromolecules* **1988**, *21*, 736.
(15) Rader, A. J.; Hespenheide, B. M.; Kuhn, L. A.; Thorpe, M. F. *Proc. Natl. Acad. Sci. U.S.A.* **2002**, *99*, 3540.
(16) Plimpton, S. J. *J. Comput. Phys.* **1995**, *117*, 1.
(17) Liu, J. W.; Mackay, M. E.; Duxbury, P. M. *Europhys. Lett.* **2008**, *84*, 46001.
(18) Mondello, M.; Yang, H.-J.; Furuya, H.; Roe, R.-J. *Macromolecules* **1994**, *27*, 3566–3574.
(19) Lyulin, A. V.; Michels, M. A. J. *Macromolecules* **2002**, *35*, 1463–1472.
(20) Lyulin, A. V.; Vorselaars, B.; Mazo, M. A.; Balabaev, N. K.; Michels, M. A. J. *Europhys. Lett.* **2005**, *71*, 618–624.
(21) Vorselaars, B.; Lyulin, A. V.; Michels, M. A. J. *Macromolecules* **2007**, *40*, 6001–6011.
(22) Lyulin, A. V.; Michels, M. A. J. *Phys. Rev. Lett.* **2007**, *99*, 085504.
(23) Weiner, S. J.; Kollman, P. A.; Case, D. A.; Singh, U. C.; Ghio, C.; Alagona, G.; Profeta, S.; Weiner, P. *J. Am. Chem. Soc.* **1984**, *106*, 765–784.
(24) Weiner, S. J.; Kollman, P. A.; Nguyen, D. T.; Case, D. A. *J. Comput. Chem.* **1986**, *7*, 230–252.
(25) Cornell, W. D.; Cieplak, P.; Bayly, C. I.; Gould, I. R.; Merz, K. M.; Ferguson, D. M.; Spellmeyer, D. C.; Fox, T.; Caldwell, J. W.; Kollman, P. A. *J. Am. Chem. Soc.* **1995**, *117*, 5179–5197.
(26) Duan, Y.; Wu, C.; Chowdhury, S.; Lee, M. C.; Xiong, G.; Zhang, W.; Yang, R.; Cieplak, P.; Luo, R.; Lee, T.; Caldwell, J.; Wang, J.; Kollman, P. *J. Comput. Chem.* **2003**, *24*, 1999–2012.
(27) Yang, L.; Tan, C.-H.; Hsieh, M.-J.; Wang, J.; Duan, Y.; Cieplak, P.; Caldwell, J.; Kollman, P. A.; Luo, R. *J. Phys. Chem. B* **2006**, *110*, 13166–13176.
(28) Han, J.; Boyd, R. H. *Polymer* **1996**, *37*, 1797–1804.
(29) Rottach, D. R.; Curro, J. G.; Grest, G. S.; Thompson, A. P. *Macromolecules* **2004**, *37*, 5468–5473.
(30) Rubinstein, M.; Colby, R. H. *Polymer Physics*; Oxford University Press: New York, 2003.
(31) Grest, G. S.; Kremer, K.; Duering, E. R. *Europhys. Lett.* **1992**, *19*, 195–200.
(32) Jacobs, D. J.; Rader, A. J.; Kuhn, L. A.; Thorpe, M. F. *Proteins: Struct., Funct., Genet.* **2001**, *44*, 150–165.